Journal of Porous Materials
https://doi.org/10.1007/s10934-024-01611-x

Efficient and low-cost mesoporous magnetic carbon composites derived from date palm stones for environmental remediation of hexavalent chromium

Shaimaa K. Mohamed[1] · Ahmed Shahat[1] · Mostafa Atito[1] · Rasha M. Kamel[1]

Accepted: 2 April 2024

Abstract
This study was performed to achieve two important scientifically challenging goals, environmental remediation of toxic heavy metals and utilization of agricultural lignocellulosic wastes. In this work, a series of mesoporous magnetic carbon (MMC) adsorbents were synthesized by carbothermic reduction at different temperatures employing date palm (Phoenix dactylifera L.) stones as the carbon source. The synthesized adsorbents were characterized by different technquies and the results confirmed the presence of zero-valent iron (ZVI) nanoparticles and other iron oxides as products of the carbothermal reduction. The nature of phases present, crystallite size and the surface properties were found to be dependent on the calcination temperature. The adsorbent MMC700 exhibited the smallest (ZVI) crystallite size 36 nm and the largest S_{BET} 341 m^2/g. All adsorbents showed mesoporous structure with mesopore average diameter lower than 6 nm. The performance was evaluated in the removal process of toxic Cr(VI) in an aqueous medium, and the optimum conditions of the process were reported. The removal process was dependant of solution pH where best results was achieved at pH = 2. Complete removal of chromium was achieved in less than 5 min by MMC700. The results were better fitted with pseudo-second-order kinetics and followed the Freundlich model isotherm. The maximum adsorption capacity was found to be 265.25 mg/g for MMC700, suggesting its application as an efficient, low-cost, and easily separable adsorbent for the toxic Cr(VI) removal process. The prepared adsorbents exhibited superior performance in the removal process compared to other agricultural wastes or biomass - derived adsorbents reported in literature.

Keywords Magnetic carbon · Date palm stone · Cr(VI) removal · Zero-valent iron · Lignocellulosic wastes · Carbothermic reduction

1 Introduction

Decreasing water sources pollution is considered crucial and vital demand for the sustainability of life; especially the aqueous pollution due to toxic heavy metals emerging from industrial effluents [1–6]. Toxic hexavalent chromium is one of the top-priority heavy metal pollutants in wastewater because of its severe effects on human health, such as liver damage, pulmonary congestion, vomiting, and severe diarrhea [7]. The permissible concentration of Cr(VI) as recommended by World Health Organization should not exceed 0.05 mg/L in drinking water [8, 9]. Conventional methods such as chemical precipitation [10], ion exchange [11], reverse osmosis [12], and adsorption [1, 2, 7, 13–15] have been used to remove chromium ions from different matrices. Among these techniques, reductive adsorption has been widely used due to its great removal capacity and easy operation where Cr(VI) is reduced to Cr(III) with subsequent adsorption [16–18]. Iron containing adsorbents has proved rapid and effective removal of Cr(VI) combined with the advantage of easy magnetic separation, especially zero-valence iron (ZVI), due to its strong reducing ability [19, 20]. The problems with (ZVI) originate from its poor air stability, agglomeration, and dissolution in acidic solutions [19]. Proper support has been reported to fix these problems and improve removal efficiency [6, 16]. Various

✉ Shaimaa K. Mohamed
Shaimaa.Mohamed@Sci.suezuni.edu.eg

[1] Department of Chemistry, Faculty of Science, Suez University, Suez, Egypt

Published online: 23 April 2024

carbon supports or composites have been widely reported in the literature due to their availability, chemical stability, and high adsorption capacity [21, 22]; however, scientific research efforts continued to provide new carbon sources with better properties or lower cost.

Carbon derived from lignocellulosic biomass and agricultural wastes can be considered a potential candidate regarding the cost-effectiveness of the process through solving the problems of both waste disposal and heavy metal pollution [23–29]. Sunkar et al. [30] utilized activated corn leaf carbon in the removal of acid blue dye 113 with adsorption capacity reaching 336 mg/g while palm shell activated carbon was used in acenaphthene and naphthalene removal from aqueos solutions [31, 32]. Date palm (Phoenix dactylifera L.) stones (also called pits or seeds) are receiving attention nowadays among agricultural wastes due to their high carbon content, low price, and wide availability [33, 34]. The chemical composition of the date stones consists mainly of carbohydrates (55–65%) and crude fiber (10–20%), while the other minor components include: oil, protein, moisture, and ash. The crude fiber and carbohydrates are composed of 23% hemicellulose, 15% lignin, 57% cellulose, and 5% ash [33]. Low-cost carbons derived from date pits biomass were applied successfully for the adsorption of various organic and inorganic contaminants from water [33]. Recently, Kumar et al. [35] used raw and modified date palm fiber in phenol adsorption and reported adsorption capacites reaching 89.67 mg/g.

In this study, a series of mesoporous magnetic carbon adsorbents were fabricated by using date palm stones as the carbon source and ferric nitrate as the iron source. The carbothermic reduction in the nitrogen atmosphere was used as the synthesis method. The synthesized magnetic carbons were studied in Cr(VI)removal, and the optimum conditions of the process were reported.

2 Materials and methods

2.1 Materials

Date palm stones (DPS) were collected from dates in Egypt. Ferric nitrate nonahydrate ($Fe(NO_3)_3.9H_2O$)(> 99.95%) was purchased from Sigma Aldrich. Ethanol (94%), Potassium dichromate ($K_2Cr_2O_7$, 99.5%), and 1,5-diphenylcarbazide(98%) were purchased from Alfa Aesar Company. Sulphuric acid (H_2SO_4, 99%) and sodium hydroxide (NaOH, 97%) was obtained from Fisher Scientific.

2.2 Preparation of milled date palm stones (MDPS)

Date palm stones (DPS) were washed well with water and dried in the air. Then, it was baked in the oven at 200°C for 25 min. The baked stones were grinded by porcelain laboratory mortar to fine powder less than 1 mm.

2.3 Synthesis of mesoporous magnetic carbon adsorbents (MMC)

The mesoporous magnetic carbon adsorbents (MMC) were synthesized by the carbothermic reduction method at different calcination temperatures. 10 g of MDPS was added to 50 mL ethanol containing 10 g of the dissolved $Fe(NO_3)_3.9H_2O$. The mixed suspension was stirred for 2 h at room temperature and then heated in a water bath at 50°C to completely evaporate ethanol to obtain ($Fe(NO_3)_3$/MDPS) solid, which was left to dry in vacuum. The impregnated solid was loaded in a tube furnace and calcined at 600, 700, or 800°C at a heating rate of 10 °C per minute under a nitrogen atmosphere and then allowed to cool. The range of calcination temperature was selected based on the data obtained from thermal analyses. The obtained solids were MMC600, MMC700, and MMC800, corresponding to the preparation calcination temperatures of 600, 700, and 800 °C, respectively. A summary of the synthesis process is given in Fig. 1.

For comparison purposes and to study the effect of the reduction process of Cr(VI) on the removal efficiency, other samples containing only the pure precursors were prepared by the above-mentioned method and calcined at 700°C. The samples were named (DS) for the calcined date palm stones and (FN) for the calcined iron salt.

2.4 Cr(VI) removal experiments

The stock solution of 1000 ppm of potassium dichromate was prepared. The chromium will be detected by Shimadzu UV2600 UV-Vis spectrophotometer using a solution of 1,5-diphenylcarbazide as a ligand [20].

The calibration curve was done between absorbance at 540 nm and chromium concentration. It fits linear to Beer-Lambert law Eq. (1):

$$A = \varepsilon 1C \tag{1}$$

where A is the absorbance, ε is absorption coefficient, l is the optical path length (cm), and C is the concentration of the analyzed solution.

The effects of pH, adsorbent weight, Cr concentration, and reaction temperature were studied. The pH was adjusted using two solutions of 1 molar from NaOH and H_2SO_4. All

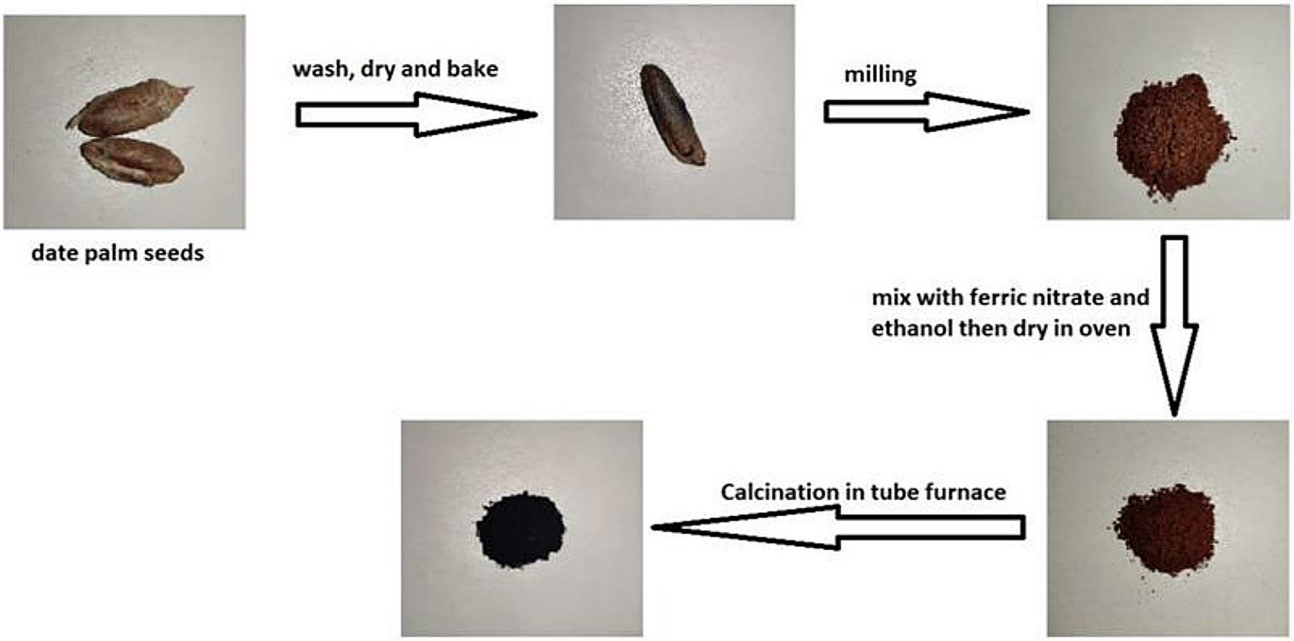

Fig. 1 The synthesis process of the mesoporous magnetic carbon adsorbents

experiments were repeated for three times. Removal kinetics and adsorption isotherms were investigated.

The Cr(VI) removal percentage (R%) was calculated by Eq. (2):

$$R\% = (C_0 - C_e)/C_0 * 100 \quad (2)$$

where C_0 and C_e (ppm) are the chromium concentrations in the solution before and after adsorption, respectively. The adsorption capacity (Q, mg/g) was measured using Eq. (3):

$$Q = (C_0 - C_e) * V/m \quad (3)$$

where V (L) is the volume of Cr(VI) solution and m (g) is the mass of the adsorbent.

2.5 Characterization

The powder XRD analysis of the samples was carried out on a Panalytical Empyrean X-Ray Diffractometer operating with a Cu-Kα radiation source (30 mA, 40 KV). Energy-dispersive X-ray spectroscopy (EDX) was carried out on JCM-6000PLUS. The Brunauer–Emmett–Teller (BET) surface area and pore size distribution were measured on a Quanta chrome Nova 3200 by nitrogen adsorption at 77.3 K. Before each measurement, the synthesized magnetic carbon samples were degassed at 200°C for 3 h under high vacuum (0.086 mPa). The pore size distribution of the samples was calculated by the Barrett–Joyner–Halenda (BJH) method using nitrogen desorption isotherms. Thermal analysis techniques were performed on a TA Instruments SDT Q600 thermogravimetric analyzer at a heating rate of 10 K/min in a nitrogen atmosphere. The magnetic properties of the powders were measured at room temperature using a vibrating sample magnetometer (VSM) Lakeshore 7410. The morphology of the adsorbent was investigated using field emission scanning electron microscopy (Zeiss FESEM Ultra 60) operated with 10 kV. The infrared spectra were obtained by (Bruker ALPHA II FT-IR) spectrophotometer employing the ATR technique. The pH at the point of zero charge (pH_{PZC}) was obtained from batch equilibrium technique where the adsorbent was dispersed in 0.01 M NaCl solution at a givin initial pH. After 48 h, the final pH was measured and pH_{PZC} was determined from the final pH – initial pH plot.

3 Results and discussion

3.1 Chemical, structural, morphological, and surface characteristics of the prepared composites

Thermal analyses curves of the precursor ($Fe(NO_3)_3$/ MDPS) are represented in Fig. 2. Two weight loss steps appeared in the thermogravimetric analysis (TG) curve; the first step is from room temperature up to 400°C, representing 57.55% of the total weight loss and the other step is from 400°C to 1000°C representing 17.28% of the total weight loss. The differential thermogravimetry (DTG) curve showed two endothermic peaks at 293.4° C and 618.4° C. The endothermic enthalpy changes calculated from differential scanning

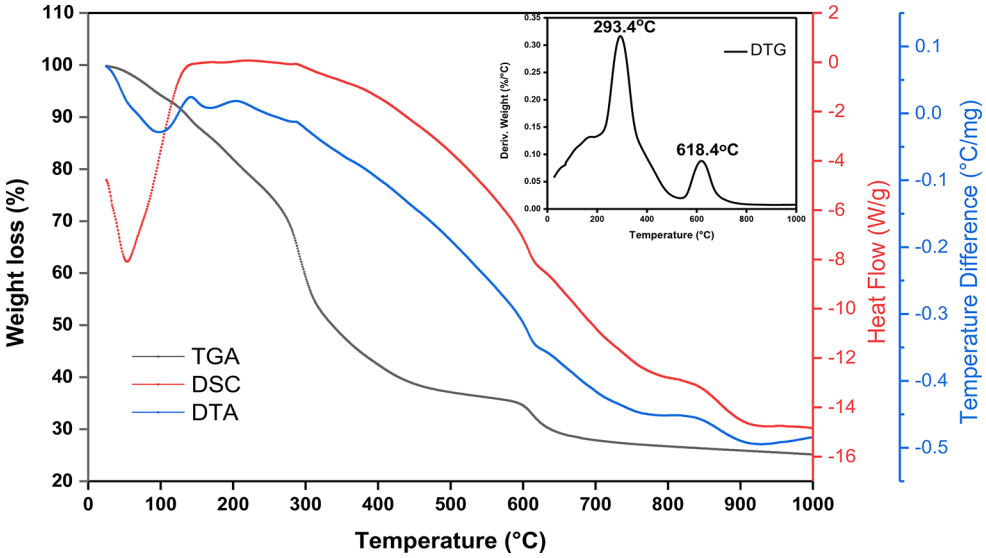

Fig. 2 Thermal analyses of the $(Fe(NO_3)_3/$ MDPS) solid precursor

calorimetry (DSC) were 1560 J/g for the peak below 120 ° C and 35.35 J/g for the small peak around 616° C. The obtained results can be explained by comparing previous thermogravimetric studies on the decomposition of pure date palm stones and the iron(III) nitrate nonahydrate salt. The pyrolysis process of the date palm stones can be divided into four stages: moisture evaporation, hemicellulose decomposition, cellulose decomposition, and lignin degradation. Nasser et al. [36] conducted a thermo-gravimetric study on different anatomical parts of the date palm, and their results revealed the decomposition temperature ranges to be 260–340 ° C for hemicellulose ($[C_5(H_2O)_4]_n$), 320–380 ° C for cellulose ($[C_6(H_2O)_5]_n$) and 300–580 °C for lignin ($[C_{10}H_{12}O_3]n$). The gaseous products of the decomposition processes included CO_2, CO, CH_4, H_2O, and a few other organics [37]. As for the decomposition of the iron salt, a two-step process occurring below 200°C was reported, which included the formation of ferric oxyhydroxide followed by the formation of Fe_2O_3 [38, 39]. Thus, the decomposition process of the precursor can be discussed as follow: (i) removal of loosely bonded water and formation of the iron oxide Fe_2O_3; (ii) decomposition of hemicellulose and cellulose, which resulted in the formation of carbon and gaseous products; (iii) reduction of $Fe_2O_3$with CO and the formation of Fe_3O_4 according to the equation:

$$3\,Fe_2O_3 + CO \rightarrow 2Fe_3O_4 + CO_2 \quad (4)$$

(iv) lignin degradation occurs over a wide range of temperatures with a further reduction of Fe_3O_4 to zero-valent iron particles by CO in a multistep process [40, 41]. The following reactions occur in the carbonization process:

$$CO + Fe_3O_4 \rightarrow 3FeO + CO_2 \quad (5)$$

$$FeO + CO \rightarrow Fe + CO_2 \quad (6)$$

$$Fe_3O_4 + 4CO \rightarrow 3\,Fe + 4\,CO_2 \quad (7)$$

(v) At high temperatures, carbon could also react with Fe_2O_3 and Fe_3O_4, which can be represented by the Eqs. (8,9):

$$C + 3\,Fe_2O_3 \rightarrow 2\,Fe_3O_4 + CO \quad (8)$$

$$C + Fe_3O_4 \rightarrow 3FeO + CO \quad (9)$$

The obtained thermogravimetric results revealed that the weight loss was slight at 600°C and negligible above 800°C, thus, three calcination temperatures were selected based on the temperature range from 600 to 800°C.

In order to investigate the composition and nature of phases present at each calcination temperature, X-ray powder diffraction was performed, and the obtained diffractograms are in Fig. 3. The sample MMC600 showed two peaks characteristic of zero-valent iron at 44.7° and 65.1°, which can be indexed to the (1 1 0) and (2 0 0) planes of Fe with cubic crystal system and space group Im-3 m. Also, four diffraction peaks located at 30.1°, 35.4°, 57.0°, and 62.6° were observed and indexed to the (2 2 0), (3 1 1), (5 1 1), (4 4 0) planes of Fe_3O_4, respectively. Raising the calcination temperature up to 700°C led to the diminishment of the Fe_3O_4 phase due to spontaneous reduction by the degradation products of date palm seeds as represented by Eqs. (5–9), yielding zero-valent iron. The presence of FeO phase as an intermediate compound in the reduction process at 700°C was confirmed by the existence of three peaks at 36.2°, 42.0°and 61.1° corresponding to (1 1 1), (2 0 0), and (2 2 0) planes of FeO. However, with a further increase of the calcination temperature to 800°C, the FeO phase disappeared, yielding zero-valent iron (ZVI) as the final product

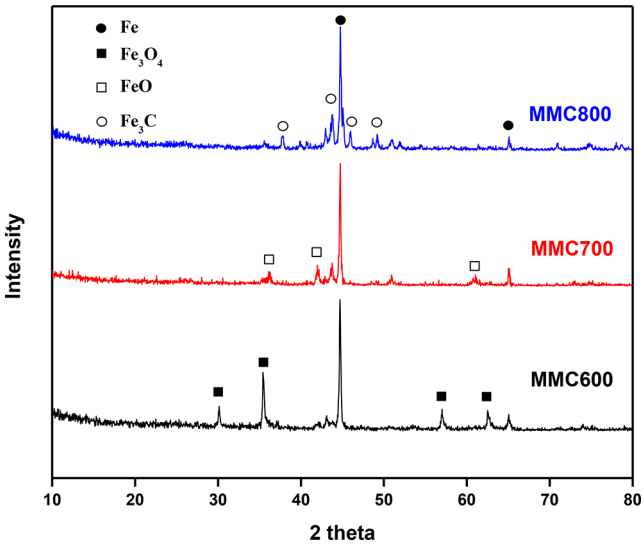

Fig. 3 XRD diffractograms of the prepared MMC adsorbents calcined at different temperatures

Table 1 Phases present, calculated crystallite size and degree of crystallinity of the prepared MMC adsorbents

Sample	Phases	Crystallite size (nm)	Degree of crystallinity
MMC600	Fe	51.99	270.98
	Fe_3O_4	50.47	107.84
MMC700	Fe	35.63	200.68
	FeO	18.57	27.90
	Fe_3C	24.41	34.58
MMC800	Fe	67.24	261.36
	Fe_3C	51.82	69.22

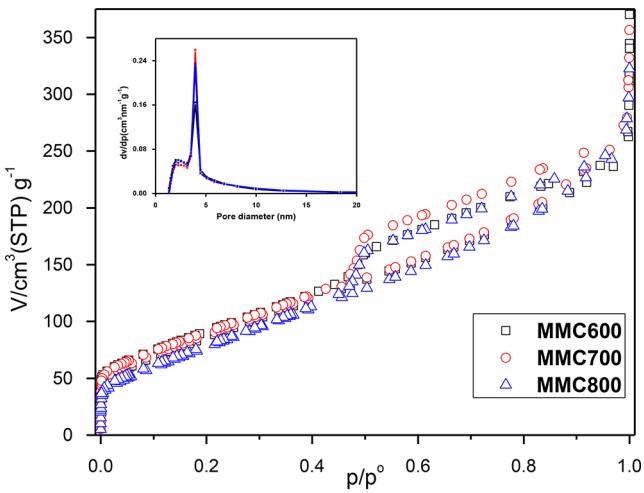

Fig. 4 Nitrogen adsorption-desorption isotherms and (insets) pore size distribution curves

of the reduction process. Fe_3C phase was observed at calcination temperatures 700 and 800ºC and characterized by diffraction peaks at 37.8°, 42.9°, 46.0°, and 49.2° where the intensity of the peaks was enhanced by increasing the calcination temperature. The Fe_3C phase could be formed due to the regional dissolution of carbon atoms into the crystal lattice of zero-valent iron [21]. No diffraction peaks of carbon appeared in the prepared samples due to their amorphous nature. Table 1 summarized the phases present in each sample and the calculated crystallite size, which was in the nano-sized range. The prepared samples are expected to be efficient in the removal process since they contained (ZVI), which is crucial in reducing toxic Cr^{6+}.

The N_2 adsorption–desorption isotherms for the MMC adsorbents (Fig. 4) showed type- IV isotherms according to IUPAC classification with Type H3 hysteresis loops in the (P/P^0) range of 0.4–0.98. This indicated the presence of slit-shaped pores, mainly in the mesopore range. Pore size distribution curves (insets Fig. 4.) showed a sharp peak at pore width 3.9 nm, which again confirmed the mesoporous nature of the pore structure with small fraction of pores in the microporous range. The surface and textural properties are summarized in Table 2, which revealed the following: (i) The value of the specific surface area was slightly increased by raising calcination temperature from 600 to 700 °C, probably due to the creation of new pores as a result of the continuous reduction process. (ii) lowering in the value of S_{BET} at 800 °C might be due to sintering and collapse of the pore structure. The difficulty in maintaining the pore structure might originate from increasing the crystallite size of (ZVI) by increasing the calcination temperature from 700 to 800ºC as evident the XRD result accompanied by the great reduction of carbon content by calcination at 800ºC (Table 3). Liang et al. [42]. , in their review of carbon-based nano zero valent iron asserted that although high calcination temperature is critical for carbothermal reduction since it is beneficial to form Fe^0 and amorphous carbon, however, the pore structure may collapse, and the specific surface area of the carbon-based material may be reduced. Different studies reported in literature [43–45] also documented the decrease in surface area at higher calcination temperatures as a result of decreasing carbon content and collapsing of the pore structure in accordance with the present work. (iii) MMC700 possessed the highest values of total pore volume and average pore diameter.

The energy dispersive X-rays' analysis was performed, and the calculated element's mass and atomic percent were

Table 2 Surface characteristics of the prepared MMC adsorbents

Sample	S_{BET} ($m^2\ g^{-1}$)	V_P ($cm^3\ g^{-1}$)	Average diameter (nm)
MMC600	335.54	0.39	4.88
MMC700	341.02	0.42	6.08
MMC800	310.93	0.41	5.49

Table 3 Elemental composition of the prepared MMC adsorbents as determined from EDX.

Element	MMC600		MMC700		MMC800	
	Mass (%)	Atom (%)	Mass (%)	Atom (%)	Mass (%)	Atom (%)
C	44.94	75.39	41.78	74.31	8.13	28.7
O	5.29	6.66	3.58	4.78	0.81	2.14
Fe	49.77	17.95	54.64	20.90	91.07	69.17

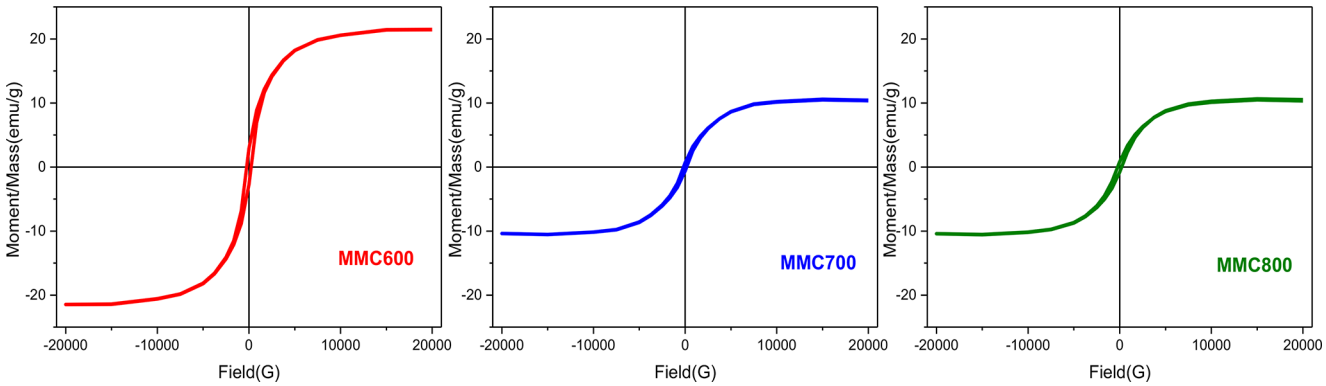

Fig. 5 Magnetic hysteresis loop of MMC adsorbents

Fig. 6 SEM image of MMC700.

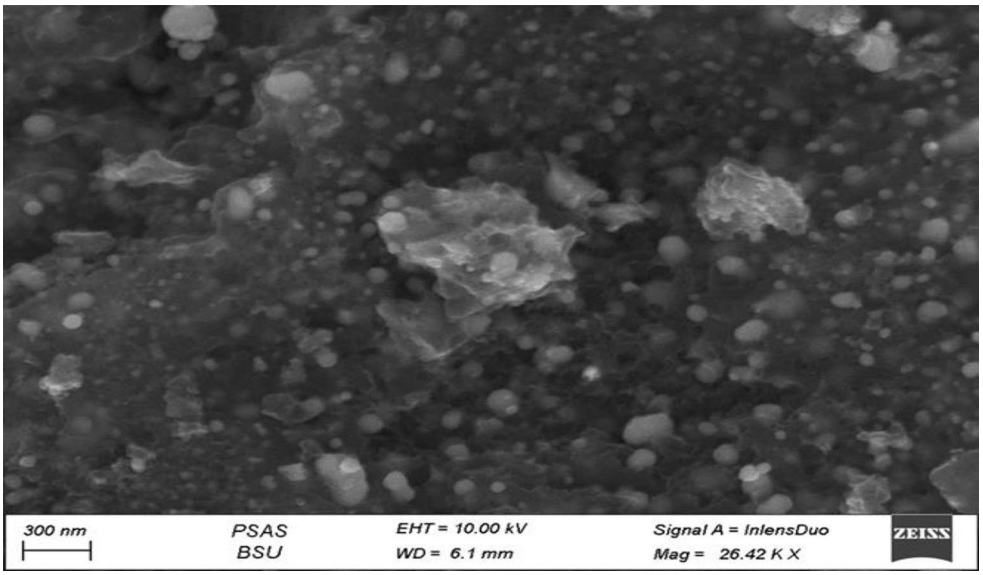

presented in Table 3. The amount of carbon was greatly reduced by raising the calcination temperature up to 800°C due to its consumption in the continuous reduction process leading to the formation of CO_2 gas. MMC800 showed the highest iron content which is the essential active component in this adsorption.

The magnetic properties of the prepared adsorbents were studied by VSM, and the results are shown in Fig. 5. The saturation magnetization values were 21.48, 10.56, and 10.60 emu/g for MMC600, MMC700, and MMC800, respectively. It was decreased by increasing the calcination temperature. The prepared samples can be easily separated magnetically from the aqueous solutions. The morphology of one selected sample, MMC700, was revealed by the SEM image in Fig. 6. Small spherical nanosized particles of ZVI can be seen in the carbon matrix.

3.2 Cr(VI) removal

3.2.1 Optimum condition for the adsorption process

The effect of calcination temperature on the removal percentage of Cr^{6+} was given in Fig. 7 as a function of time. Complete removal was noticed after only 5 min for the samples calcined at 700 and 800°C, suggesting their application as a promising candidate for removing toxic Cr^{6+} from an aqueous environment. The sample MMC700 was subjected to further study due to: (i) complete removal of toxic Cr^{6+}

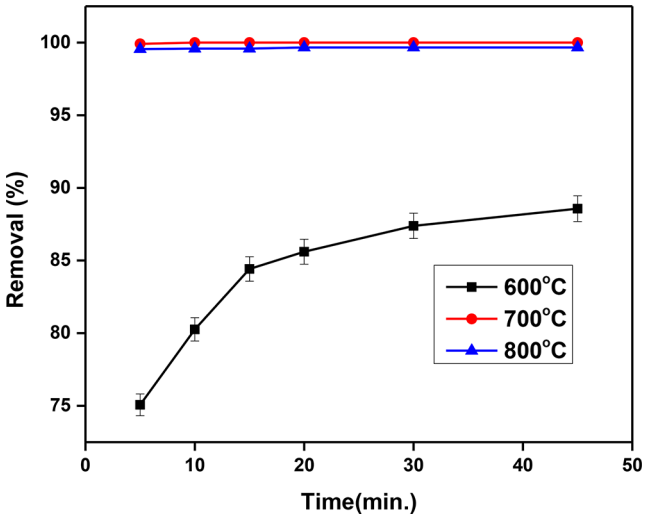

Fig. 7 The effect of calcination temperature on the removal capacity of Cr^{6+} performed at 25 °C. The adsorption conditions were: pH = 2, solution volume = 100 ml, concentration of Cr^{6+} = 50 ppm, and dose = 0.05 g

from the aqueous solution; (ii) higher specific surface area value relative to other prepared samples, and (iii) saving energy by performing the calcination at 700°C instead of 800°C.

The effect of different reaction conditions on the removal percentage of Cr^{6+} by MMC700 was shown in Fig. 8.

3.2.1.1 Effect of pH The study of different pH values on the adsorption process revealed that complete removal of Cr^{6+} could be achieved at pH = 1 and pH = 2; therefore, pH = 2 was taken as the optimum pH for further adsorption and kinetic studies. With increasing the pH value, the removal efficiency decreased, which is a common behavior in Cr^{6+} reductive adsorption process [19, 20]. The reason for this behavior is related to the charges on the surface of adsorbent and the chemistry of chromium ions in solution and its dependence on the pH [6, 8]. The pH_{pzc} of MMC700 was found to be 6.35, which indicated that the surface is positively charged below pH = 6.35 and negatively charged above that point. Thus at lower pH values the MMC700 adsorbent surface will efficiently attract anionic species. In an acidic aqueous medium (pH 1–6), Cr(VI) has $Cr_2O_7^{2-}$ and the predominant $HCrO_4^-$ forms, which are favorably adsorbed on the positively charged surface of MMC700 adsorbent. Then, the adsorbed species are easily reduced by ZVI and/ or Fe^{2+} ions forming the Cr-Fe complex, which is precipitated according to Eqs. (10–14) [20]:

$$Cr_2O_{7(aq)}^{2-} + 3Fe^0{}_{(s)} + 14\,H^+{}_{(aq)} \rightarrow 2\,Cr^{3+}{}_{(aq)} + 3\,Fe^{2+}{}_{(aq)} + 7H_2O \quad (10)$$

$$Cr_2O_{7(aq)}^{2-} + 6\,Fe^{2+}{}_{(aq)} + 14\,H^+{}_{(aq)} \rightarrow 2\,Cr^{3+}{}_{(aq)} + 6\,Fe^{3+}{}_{(aq)} + 7\,H_2O \quad (11)$$

$$2\,HCrO_4^- + 3\,Fe^0{}_{(s)} + 14\,H^+{}_{(aq)} \rightarrow 2\,Cr^{3+}{}_{(aq)} + 3\,Fe^{2+}{}_{(aq)} + 8\,H_2O \quad (12)$$

$$2\,HCrO_4^- + 6\,Fe^{2+}{}_{(aq)} + 14\,H^+{}_{(aq)} \rightarrow 2\,Cr^{3+}{}_{(aq)} + 6\,Fe^{3+}{}_{(aq)} + 8\,H_2O \quad (13)$$

$$x\,Cr^{3+}(aq) + (1-x)\,Fe^{3+}(aq) + 3\,H_2O \rightarrow Cr_xFe_{(1-x)}(OH)_3 \downarrow + 3\,H^+ \quad (14)$$

On the other hand, at pH > 6.0 chromate ions (CrO_4^{2-}) predominate the solution while the adsorbent surface became negatively charged. This leads to an electrostatic replusion between the adsorbent surface and the anionic chromate ions which resulted in decreasing the removal efficiency [8, 46].

3.2.1.2 Effect of adsorbent weight Investigation of the effect of MMC700 weight in the range of (0.01–0.10 g) on the removal percentage at pH = 2 revealed the optimum weight to be 0.05 g to achieve complete removal of Cr^{6+}. It can be seen from Fig. 8b that even using the low weight of MMC700 could achieve 99% removal, which again asserts the high efficiency of the prepared material.

3.2.1.3 Effect of Cr^{6+} solution concentration Different initial concentrations of Cr^{6+} solution were investigated (Fig. 8c), and it was shown that MMC700 could completely remove the toxic ion up to a high concentration as 200 ppm. The prepared adsorbent could remove up to 90% when the initial concentration of Cr^{6+} solution was 250 ppm; this may be due to a shortage of adsorption sites on the surface of the MMC700.

3.2.1.4 Effect of reaction temperature The effect of three different reaction temperatures (20, 25, 35 °C) on the reductive removal process was studied at two different pH. Complete removal was achieved at pH = 2 at all studied reaction temperatures. For further study of the effect, neutral pH was used, and it was concluded that the optimum reaction temperature is 25°C (Fig. 8d).

Thus, to summarize the optimal conditions for obtaining the best performance in the removal process for MMC700: Solution volume = 50 ml, concentration of Cr(VI) = 50 ppm, dose = 0.05 g, pH = 2, and reaction temperature 25°C.The performance of the prepared MMC700 in the removal process was compared to that of the pure calcined date palm seeds and the calcined iron salt in Fig. 9. It can be seen that even at natural pH, the removal capacity of the prepared composite is much higher than that of pure carbon and pure iron oxide due to a large amount of nZVI contained in the sample that is the crucial factor in the reductive adsorption of Cr^{6+}.

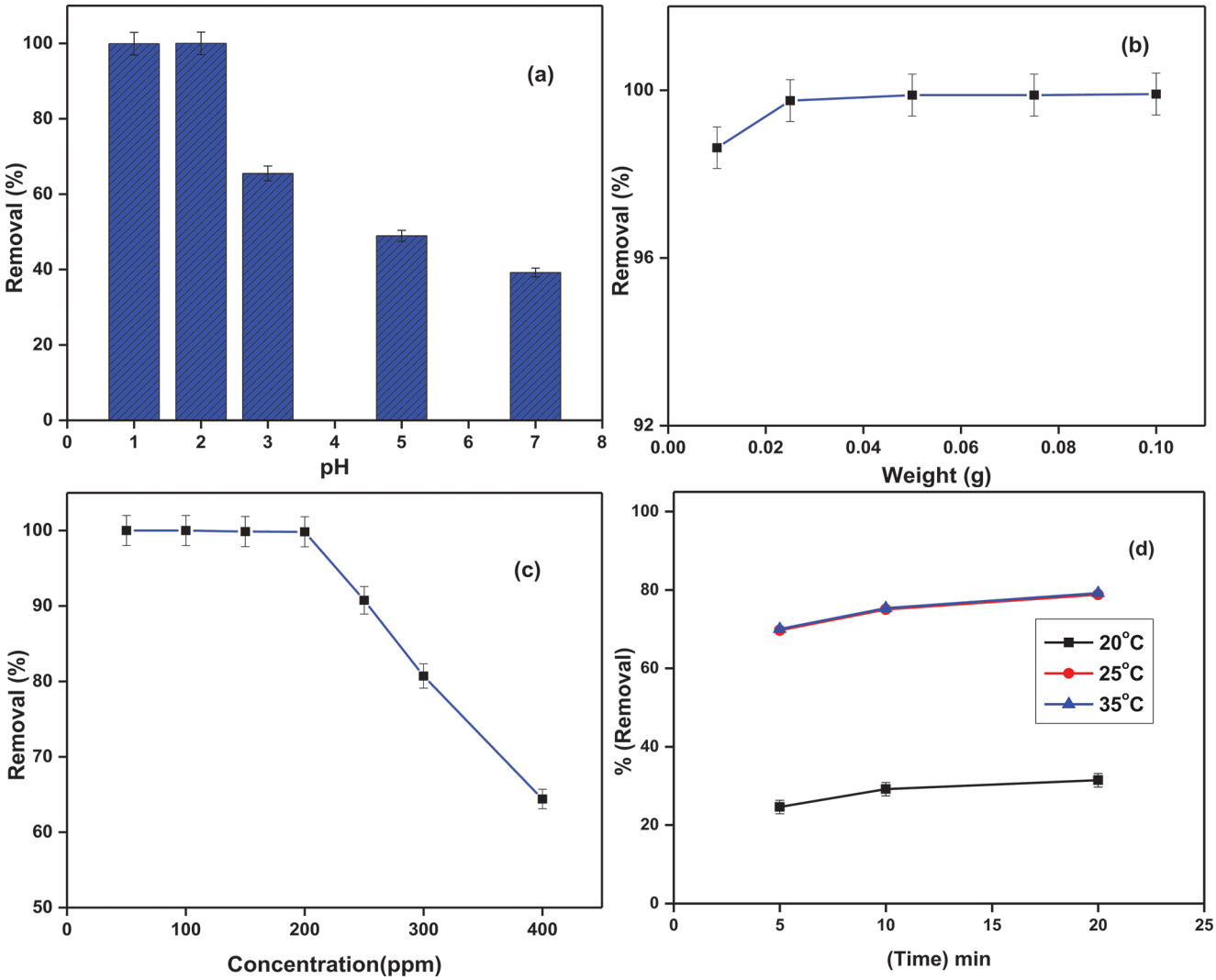

Fig. 8 The effect of different reaction conditions on the removal percentage of Cr^{6+} by MMC700. (a) The effect of different pH at 25°C (volume = 50 ml, concentration of Cr^{6+} = 50 ppm, dose = 0.05 g). (b) The effect of different adsorbent dose at 25°C (pH = 2, volume = 50 ml, concentration of Cr^{6+} = 50 ppm). (c)The effect of different concentration of Cr^{6+} solution at 25°C (volume = 50 ml, pH = 2, dose = 0.05 g). (d) The effect of reaction temperature (pH = 7, volume = 50 ml, concentration of Cr^{6+} = 4 ppm, and dose = 0.05 g)

3.2.2 Study of kinetics and adsorption isotherms

The study of the kinetics of the reductive adsorption of MMC700 sample was characterized by a very fast rate at pH = 2; complete removal of toxic Cr^{6+} ions was established in only one minute when the reaction conditions were (volume = 100 ml, the concentration of Cr^{6+} = 50 ppm, dose = 0.05 g and temperature = 25 °C). The same phenomenon was noticed for other nZVI/ carbon composites from different carbon sources reported in the literature [20]. To investigate the kinetics, different reaction conditions were used, and the obtained data were employed in the pseudo-first order model and pseudo-second order model (Fig. 10).

The pseudo first-order model is given by the following equation:

$$\ln\,(q_e - q_t) = \ln\,q_e - K_1\,t \tag{15}$$

where q_e is the equilibrium adsorption capacity (mg/g), q_t is the time-based adsorption capacity (mg/g), k_1 is the rate constant for the pseudo-first order model (min^{-1}), and t is the time (min) [47].

The pseudo second-order model is given by the following equation:

$$t/q_t = 1/k_2 q_e^{\,2} + t/q_e \tag{16}$$

where k_2 is the rate constant for pseudo-second-order model (g/mg min) [47]. The results were better fitted with pseudo-second order kinetics (Table 4), based on its highest adjusted regression coefficient (adj.R^2) value, which reveals that the

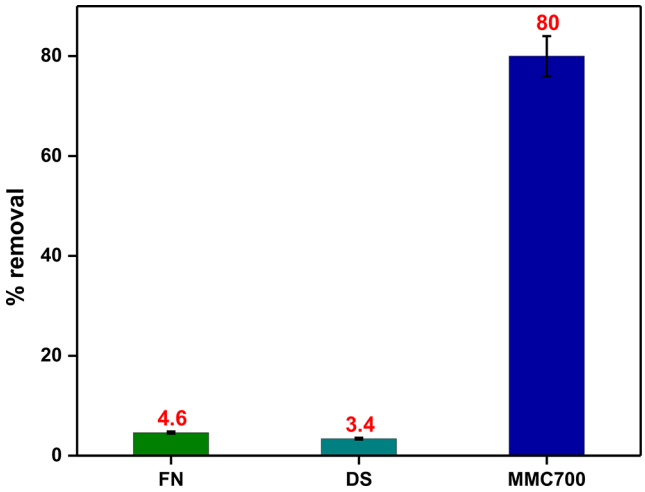

Fig. 9 Comparison between the removal percentages of (pH = 7, volume = 50 ml, concentration of Cr^{6+} = 4 ppm, and dose = 0.05 g)

reaction rate is mainly governed by chemical adsorption [20].

The adsorption isotherm was investigated by three models, namely, Freundlich, Langmuir, and Temkin, and represented by Fig. 11 through linear and nonlinear fitting. The parameters and statistics of each adsorption model were given in Table 4 to compare the better fitness of each model. All the simulations, fittings and calculations were made using the Origin Pro 9 64-bit Academic software (Origin Lab Corporation, Northampton, MA, USA).

The Freundlich isotherm, which describes non-specific adsorption involving multi-layers [20], is given by the following equation:

$$\log\ q_e = \log K_F + (1/n)\log C_e \tag{17}$$

where K_F is the Freundlich isotherm constant ($mg^{1-1/n}\ L^{1/n}$ / g) and n is the intensity factor for adsorption [33].

The Langmuir isotherm is given by the following equation [33]:

$$(1/q_e) = (1/Q_{max}K_L C_e) + (1/Q_{max}) \tag{18}$$

where Q_{max} is the theoretical maximum of monolayer adsorption capacity (mg/g) and K_L is the Langmuir isotherm constant (L/mg).

The Temkin isotherm is given by the following equation [33]:

$$q_e = (RT/b)\ln K_T + (RT/b)\ln C_e \tag{19}$$

where R is the universal gas constant (J/mol K), T is the adsorption temperature (K), b is the bonding factor related to the heat of adsorption (J/mol), and K_T is the Temkin isotherm constant (L/g).

The fitting quality of the models was judged by the values of the adjusted regression coefficient (Adj.R^2), the residual sum of squares (RSS), and the reduced chi-squared parameter (Red. $\chi 2$). High (RSS) and (Red. $\chi 2$) values indicated a high bias between the experimental data and the tested model and consequently the unfitness of the model while higher values of (Adj.R^2) indicated good fitting [30, 31, 48, 49]. It can be seen from Table 4 that: (i) there was no significant difference between the computed values of parameters by linear or nonlinear fitting. (ii) Freundlich model satisfied the high value of (Adj.R^2) and have the lowest error in (RSS) and (Red. $\chi 2$) values. Thus, the obtained data were found to fit the Freundlich model, which considers the heterogeneous adsorptive energies on the surface of the adsorbent. The

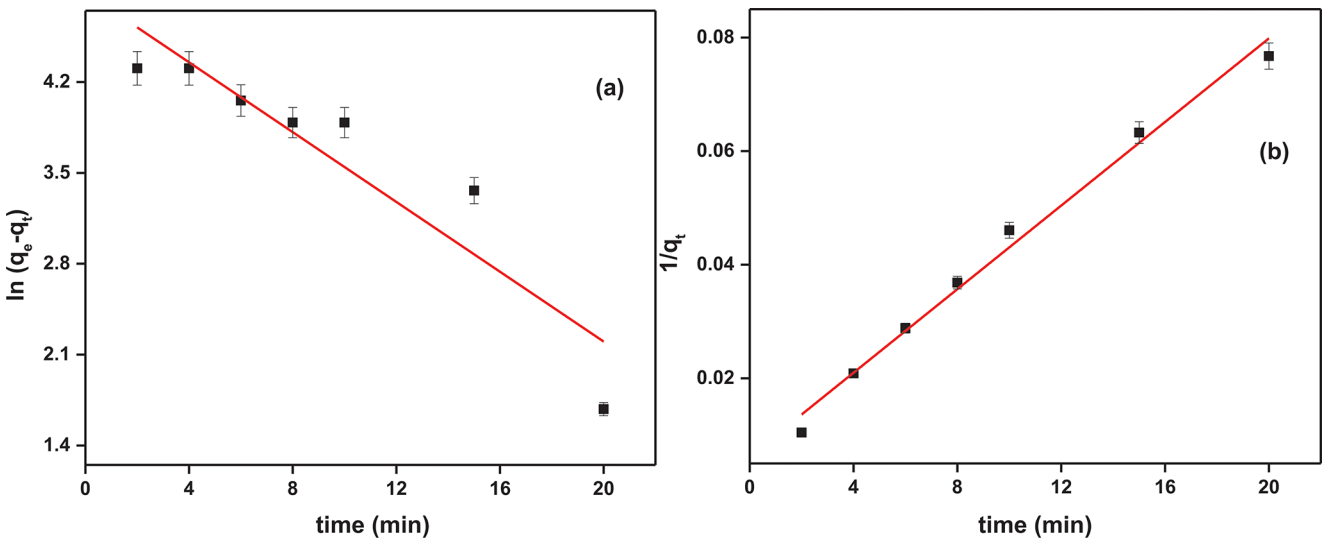

Fig. 10 (a) Pseudo first order kinetics and (b) pseudo second order kinetics

Table 4 Parameters obtained from different adsorption isotherms and kinetic models and corresponding regression statistics

Model	Fitting	Parameters		Statistics		
		Parameter	Value	Adj R^2	Rss	Red. χ^2
Langmuir	NL	Q_{max} (mg/g)	265.79	0.9978	88.485	22.1214
		K_L (L/mg)	0.2336			
	L	Q_{max} (mg/g)	265.25	0.8858	$2.16*10^{-8}$	
		K_L (L/mg)	0.2441			
Freundlich	NL	1/n	0.0748	0.9887	7.690	2.5634
		$K_F(mg^{1-1/n}\ L^{1/n}/g)$	178.86			
	L	1/n	0.0745	0.9899	$2.14*10^{-5}$	
		$K_F(mg^{1-1/n}\ L^{1/n}/g)$	179.171			
Temkin	NL	b (J/mol)	135.757	0.9997	10.446	2.6116
		K_T (L/g)	10334.23			
	L	b (J/mol)	135.747	0.9847	10.446	
		K_T (L/g)	10334.24			
Pseudo-first Order	L	q_e (mg/g)	123.843	0.8268	0.7364	
		$k_1 \times 10^{-3}$ (min^{-1})	6.543			
Pseudo-second Order	L	q_e (mg/g)	270.27	0.9878	$3.35*10^{-5}$	
		$k_2 \times 10^{-3}$ (g/mg min)	2.385			

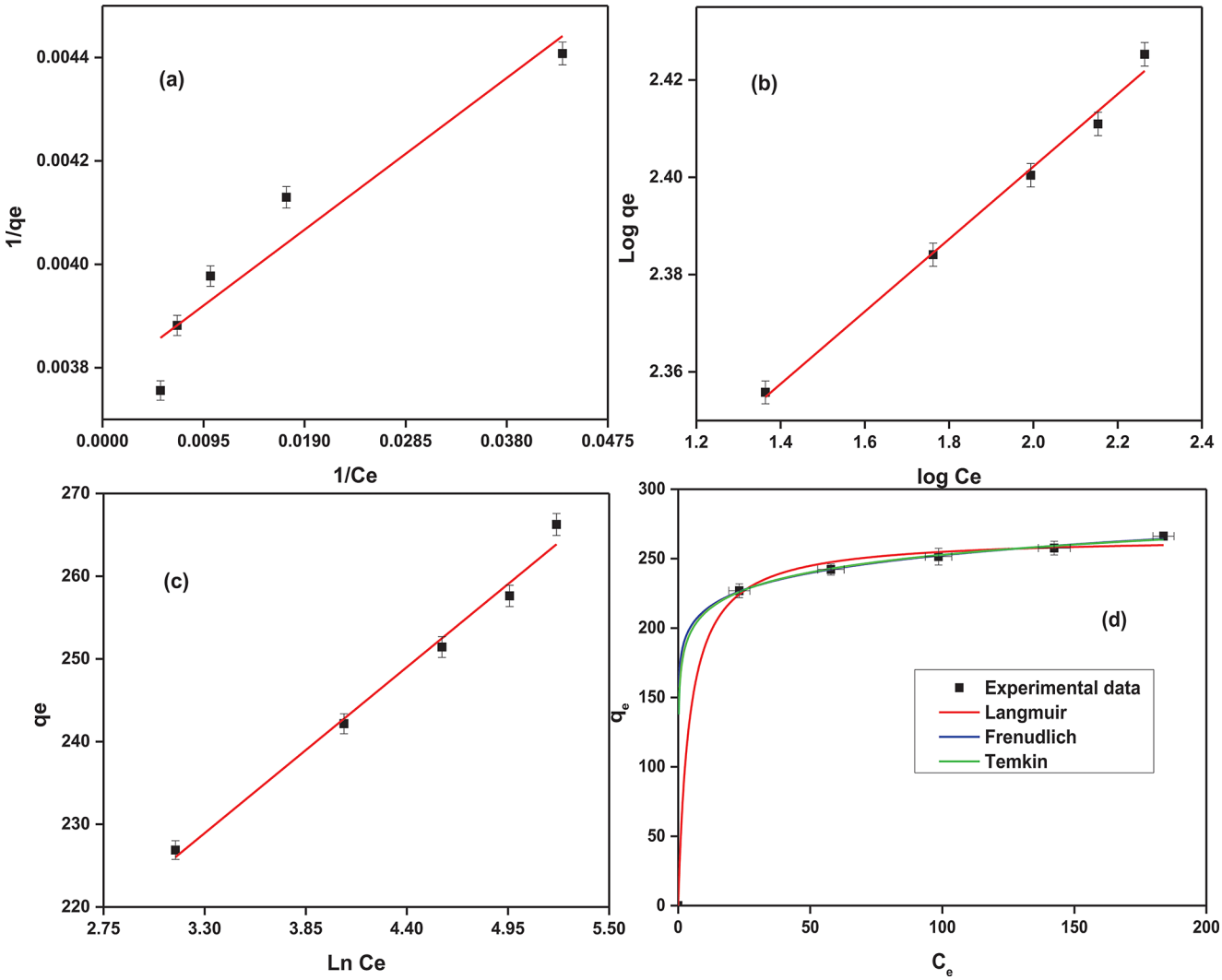

Fig. 11 Linear Fitting of adsorption isotherms (a) Langmuir, (b) Freundlich, and (c) Temkin. Non linear fitting of adsorption isotherms (d)

value of 1/n ($<<1$) indicated a chemisorption process and confirmed the high heterogeneity of the adsorbent surface.

3.2.3 Cr (VI) adsorption mechanism

To elucidate the adsorption mechanism of Cr (VI) by MMC700, further analyses were conducted before and after the adsorption process. XRD, and FTIR analyses were performed, and the results were presented in (Figures S1 and S2). It can be seen from Figure S1 that, the intensity of XRD peaks were reduced after the adsorption process while a small broad peak appeared around $2\theta = 35.51^{o}$ which might be indexed to Fe_2O_3 (35.68), Fe_3O_4 ($2\theta = 35.45^{o}$) and/or Cr_2FeO_4 ($2\theta = 35.50^{o}$) [50–52]. This confirmed the redox reaction between Fe^0 and Fe^{2+} species in MMC700 with Cr(VI) and formation of the Cr(III)-Fe(III) complex containing species according to Eq. (14). The FTIR spectra of MMC700 adsorbent (Figure. S2) revealed the presence of the characteristic peaks of Fe-O observed at 469 and 525 cm^{-1} [53]. The peaks at 742 and1538 cm^{-1} may be attributed to the bending and stretching vibrations of (C = C), respectively [54]. The peak at 1052 cm^{-1} assigned to the stretching vibrations of (C-O) while peaks at 2080 and 2182 cm^{-1} may be due to stretching vibrations of (C ≡ C). The small peak at 3351 cm^{-1} may be attributed to the stretching vibrations of (O-H). After Cr (VI) adsorption, new sharp peaks appeared at 3613 and 3743 cm^{-1} in the spectra assigned to stretching vibration of (O-H) may be due to formation Cr(III)/Fe(III) hydroxide-containing species [52]. The value of S_{BET} was found to decreased to 322.36 m^2/g after Cr(VI) reductive adsorption which may be attributed to the partial blocking of MMC700 mesopores by the reduction products (Fe(III) and Cr(III) containing phases). Similar behaviour was reported in literature [9, 55]. Based on the obtained results, Cr(VI) remediation by MMC700 adsorbent in acidic pH might processed through the following mechanism: (i) favourable adsorption of anionic Cr(VI) species to the positively charged MMC700 surface by electrostatic interaction. (ii) Reduction of Cr(VI) to Cr(III)-containing species by the electron-donor groups which are mainly Fe^0 and Fe^{2+} in MMC700 while carbon act as both efficient support for iron nanoparticles and excellent electron transfer mediator to promote the electron transfer process according to Eqs. (10–13). The synergistic effect between the nano-sized iron and carbon in MMC700 was proved to enhance the removal efficiency by 17-fold more than pure iron even in neutral medium (Fig. 9). (iii) co-precipitation of Cr- Fe containing species within the mesopores of MMC700.

Table 5 Comparison between Q_{max} values for chromium (VI) removal reported in literature and current study

Adsorbent	Q_{max} (mg/g)	Reference
Nano-iron active carbon composites	187.11	[57]
Magnetite functionalized nigella sativa seeds	10.21	[58]
Activated iron bamboo biochar	25.68	[59]
Magnetite-pine composite	15.24	[60]
Starch functionalized iron oxide nanoparticles	9.02	[61]
Starch functionalized magnetite nanoparticles	26.60	[62]
Magnetic carbon nanocomposites (cotton)	3.74	[63]
N-doped porous carbon with magnetic particles (rice husk)	16.00	[64]
Amino-functionalized magnetic cellulose nanocomposite	171.50	[65]
iron nanoparticles embedded in orange peel pith	5.37	[66]
Cellulose derived magnetic mesoporous carbon nanocomposites	327.50	[20]
iron-based solid wastes composite	393.79	[56]
Biochar-anchored low-cost natural iron-based composites	81.50	[67]
Epigallocatechin gallate/titanium composites	105.80	[68]
MMC700	265.25	This study

3.2.4 Comparison with other adsorbents and practical feasibility

The calculated maximum Cr(VI) removal capacity from the Langmuir model was 265.25 mg/g. Comparison with reported literature for magnetic carbons derived from natural or synthetic sources (Table 5) revealed the excellent activity of the prepared MMC700 and suggested its application as an efficient candidate for Cr (VI) remediation purposes. Although Qi et al. [56] reported higher adsorption capacity for the composite prepared from iron-based solid wastes, but their measurments were conducted over 1200 h while maximum of 2 h were used in our work. The practical feasibility of the prepared MMC700 adsorbent was elucidated by studying its reusability and application in real water samples. The reusability was tested by treating the used adsorbent by 0.1 M NaOH solution for 2 h under continuous stirring, then washing with distilled water and finally drying at 90ºC in vacuum oven. The removal efficiency was measured for five cycles of repeated procedures and the results were presented in (Figure S3). The adsorbent maintained good removal efficiency up to three cycles, however, the removal efficiency was significantly reduced by the fifth cycle may be due to consumption of active adsorption sites. To investigate the ability of MMC700 in removal of Cr(VI) from real water samples, tap water was spiked with 50 ppm Cr(VI) and treated with the adsorbent at the predetermined optimum conditions. Tap water normally contains different dissolved ions (for example: magnesium, calcium, sodium, chloride, sulphate, and bicarbonate) which may interfere with the adsorption process. It was found that the removal efficiency was slightly reduced in spiked tap water (Figure S3). This may be attributed to the competition

of some anionic species present in tap water with chromium species for the adsorption sites on the positively charged adsorbent surface at acidic pH.

This is the first time to report the synthesis and use of this type of organic/inorganic porous hybrid materials in removal of toxic Cr(VI). The prepared adsorbents exhibited superior performance in the removal process compared to other agricultural wastes or biomass - derived adsorbents reported in literature. The relatively high specific surface area together with the mesoporous structure of the composites contributed mainly to the complete removal of the toxic metal. The obtained results open avenues for the synthesis of low-cost, efficient, and easily separable magnetic adsorbents together with the achievement of two important goals of the study: utilization of agricultural waste and minimizing heavy metal pollution.

4 Conclusions

A series of mesoporous magnetic carbon adsorbents were synthesized employing date palm (Phoenix dactylifera L.) stones as the carbon source and ferric nitrate as the iron source. The mechanism and the chemical reactions occurring during the carbothermal reduction synthesis were discussed. The effect of different carbonizing temperatures (600, 700 and 800°C) on the structural, magnetic, and surface properties of the adsorbents was studied. The presence of nano zero-valent iron was confirmed in all the prepared adsorbents while iron oxide phases was detected at calcination temperature 600 and 700°C. Surface studies elucidated the mesoporous structure of adsorbents with high values of S_{BET} reaching 341.02 m^2/g for MMC700. The saturation magnetization values were decreased by increasing the carbonizing temperature from 600 to 700°C.

The prepared adsorbents were utilized in toxic Cr(VI) remediation from aqueous medium while studying the optimum removal conditions and the adsorption mechanism. The best removal behavior was achieved by MMC700 with a very fast rate at pH = 2 and 25°C with maximum adsorption capacity 265.25 mg/g. The obtained data were found to fit the Freundlich model as a chemisorption process while high heterogeneity of the adsorbent surface was confirmed. The kinetics of removal followed pseudo second-order model. MMC700 exhibited superior performance in the removal process compared to other reported agricultural wastes or biomass - derived adsorbents with reasonable practical feasibility. The synergistic effect of carbon as excellent electron transfer mediator and nanosized (Fe^0 / Fe^{2+}) as electron donor along with the high specific surface area mesoporous structure contributed mainly to the reductive removal mechanism. The obtained results suggest the application of MMC700 as an efficient low-cost, and easily separable adsorbent for the toxic Cr(VI) removal process. Also, the prepared adsorbent might be a promising candidate for waste water purification by removal of other toxic heavy metals.

Supplementary Information The online version contains supplementary material available at https://doi.org/10.1007/s10934-024-01611-x.

Author contributions S. M.: Conceptualization, Visualization, Supervision, Writing - original draft. A. S.: Conceptualization, Resources. M. A.: Investigation, Writing - review & editing. R. K.: Supervision.

Funding No funding was received to assist with the preparation of this manuscript.
Open access funding provided by The Science, Technology & Innovation Funding Authority (STDF) in cooperation with The Egyptian Knowledge Bank (EKB).

Data availability No datasets were generated or analysed during the current study.

Declarations

Conflict of interest The authors declare that they have no known competing financial interests or personal relationships that could have appeared to influence the work reported in this paper.

References

1. L. Liu, W. Cai, C. Dang, B. Han, Y. Chen, R. Yi, J. Fan, J. Zhou, J. Wei, One-step vapor-phase assisted hydrothermal synthesis of functionalized carbons: effects of surface groups on their physicochemical properties and adsorption performance for cr (VI). Appl. Surf. Sci. **528**, 146984 (2020)
2. H. Liang, R. Sun, B. Song, Q. Sun, P. Peng, D. She, Preparation of nitrogen-doped porous carbon material by a hydrothermal-activation two-step method and its high-efficiency adsorption of cr (VI). J. Hazard. Mater. **387**, 121987 (2020)
3. U.K. Sahu, J. Chen, H. Ma, M.K. Sahu, S. Mandal, B. Lai, S. Pu, As(III) removal from aqueous solutions using simultaneous oxidation and adsorption process by hierarchically magnetic flower-like Fe3O4@C-dot@MnO2 nanocomposite. J. Environ. Health Sci. Eng. **21**, 47–61 (2023). https://doi.org/10.1007/s40201-022-00834-x

4. U.K. Sahu, M.K. Sahu, S.S. Mahapatra, R.K. Patel, Removal of as(III) from aqueous solution using Fe3O4 nanoparticles: process modeling and optimization using Statistical Design. Water Air Soil Pollut. **228**, 45 (2016). https://doi.org/10.1007/s11270-016-3224-1
5. U.K. Sahu, S. Sahu, S.S. Mahapatra, R.K. Patel, Cigarette soot activated carbon modified with Fe3O4 nanoparticles as an effective adsorbent for as(III) and as(V): material preparation, characterization and adsorption mechanism study. J. Mol. Liq. **243**, 395–405 (2017). https://doi.org/10.1016/j.molliq.2017.08.055
6. U.K. Sahu, W. Ji, Y. Liang, H. Ma, S. Pu, Mechanism enhanced active biochar support magnetic nano zero-valent iron for efficient removal of cr(VI) from simulated polluted water. J. Environ. Chem. Eng. **10**, 107077 (2022). https://doi.org/10.1016/j.jece.2021.107077
7. Y. Wang, C. Peng, E. Padilla-Ortega, A. Robledo-Cabrera, A. López-Valdivieso, Cr (VI) adsorption on activated carbon: mechanisms, modeling and limitations in water treatment. J. Environ. Chem. Eng. **8**, 104031 (2020)
8. U.K. Sahu, S. Tripathy, N. Gouda, H.S. Mohanty, M.K. Sahu, S.P. Panda, Y.M. Krishna, S. Samantaray, V.S.R. Kumar, N. Banu et al., Activated Carbon–Modified Iron Oxide nanoparticles for Cr(VI) removal: optimization, Kinetics, isotherms, thermodynamics, Regeneration, and mechanism study. Water Air Soil Pollut. **234**, 561 (2023). https://doi.org/10.1007/s11270-023-06588-y
9. U.K. Sahu, Y. Zhang, W. Huang, H. Ma, S. Mandal, S. Sahu, M.K. Sahu, R.K. Patel, S. Pu, Nanoceria-loaded tea waste as bio-sorbent for cr(VI) removal. Mater. Chem. Phys. **290**, 126563 (2022). https://doi.org/10.1016/j.matchemphys.2022.126563
10. W. Ma, J. Gao, Z. Chen, J. Hu, G. Xin, Y. Pan, Z. Zhang, D. Tan, A new method of cr (VI) reduction using SiC doped carbon electrode and cr (III) recovery by hydrothermal precipitation. Colloids Surf., a **610**, 125724 (2021)
11. J. Sánchez, D. Dax, Y. Tapiero, C. Xu, S. Willför, Bio-based Hydrogels with Ion Exchange Properties Applied to remove Cu (II), cr (VI), and as (V) ions from water. Front. Bioeng. Biotechnol. **9**, 327 (2021)
12. A. Karunakaran, A. Chaturvedi, J. Ali, R. Singh, S. Agarwal, M. Garg, Response surface methodology-based modeling and optimization of chromium removal using spiral-wound reverse-osmosis membrane setup. Int. J. Environ. Sci. Technol. 2021, 1–12
13. B. Ghanim, J.J. Leahy, T.F. O'Dwyer, W. Kwapinski, J.T. Pembroke, J.G. Murnane, Removal of hexavalent chromium (cr (VI)) from aqueous solution using acid-modified poultry litter-derived hydrochar: adsorption, regeneration and reuse. J. Chem. Technol. Biotechnol. **97**, 55–66 (2021)
14. D.-M. Liu, C. Dong, B. Xu, Preparation of magnetic kaolin embedded chitosan beads for efficient removal of hexavalent chromium from aqueous solution. J. Environ. Chem. Eng. **9**, 105438 (2021)
15. K. Ding, X. Zhou, H. Hadiatullah, Y. Lu, G. Zhao, S. Jia, R. Zhang, Y. Yao, Removal performance and mechanisms of toxic hexavalent chromium (cr (VI)) with ZnCl2 enhanced acidic vinegar residue biochar. J. Hazard. Mater. **420**, 126551 (2021)
16. Y. Wang, L. Yu, R. Wang, Y. Wang, X. Zhang, A novel cellulose hydrogel coating with nanoscale Fe0 for cr (VI) adsorption and reduction. Sci. Total Environ. **726**, 138625 (2020)
17. N.S. Alsaiari, A. Amari, K.M. Katubi, F.M. Alzahrani, F.B. Rebah, M.A. Tahoon, Innovative magnetite based polymeric nanocomposite for simultaneous removal of methyl orange and hexavalent chromium from water. Processes. **9**, 576 (2021)
18. N. Guo, X. Lv, Q. Yang, X. Xu, H. Song, Effective removal of hexavalent chromium from aqueous solution by ZnCl2 modified biochar: effects and response sequence of the functional groups. J. Mol. Liq. **334**, 116149 (2021)
19. Y. Dai, Y. Hu, B. Jiang, J. Zou, G. Tian, H. Fu, Carbothermal synthesis of ordered mesoporous carbon-supported nano zero-valent iron with enhanced stability and activity for hexavalent chromium reduction. J. Hazard. Mater. **309**, 249–258 (2016)
20. B. Qiu, H. Gu, X. Yan, J. Guo, Y. Wang, D. Sun, Q. Wang, M. Khan, X. Zhang, B.L. Weeks, Cellulose derived magnetic mesoporous carbon nanocomposites with enhanced hexavalent chromium removal. J. Mater. Chem. A **2**, 17454–17462 (2014)
21. K. Zhu, C. Chen, M. Xu, K. Chen, X. Tan, M. Wakeel, N.S. Alharbi, In situ carbothermal reduction synthesis of Fe nanocrystals embedded into N-doped carbon nanospheres for highly efficient U (VI) adsorption and reduction. Chem. Eng. J. **331**, 395–405 (2018)
22. S. Afshin, Y. Rashtbari, M. Vosough, A. Dargahi, M. Fazlzadeh, A. Behzad, M. Yousefi, Application of Box–Behnken design for optimizing parameters of hexavalent chromium removal from aqueous solutions using Fe3O4 loaded on activated carbon prepared from alga: kinetics and equilibrium study. J. Water Process. Eng. **42**, 102113 (2021)
23. S.K. Mohamed, S. Abd Elsalam, A. Shahat, H.M. Hassan, R.M. Kamel, Efficient sucrose-derived mesoporous carbon sphere electrodes with enhanced hydrophilicity for water capacitive deionization at low cell voltages. New J. Chem. **45**, 1904–1914 (2021)
24. P. Miretzky, A.F. Cirelli, Cr (VI) and cr (III) removal from aqueous solution by raw and modified lignocellulosic materials: a review. J. Hazard. Mater. **180**, 1–19 (2010)
25. A. Shakya, T. Agarwal, Removal of cr (VI) from water using pineapple peel derived biochars: Adsorption potential and reusability assessment. J. Mol. Liq. **293**, 111497 (2019)
26. Y. Wang, Q. Yang, J. Chen, J. Yang, Y. Zhang, Y. Chen, X. Li, W. Du, A. Liang, S.-H. Ho, Adsorption behavior of cr (VI) by magnetically modified Enteromorpha prolifera based biochar and the toxicity analysis. J. Hazard. Mater. **395**, 122658 (2020)
27. B. Thangagiri, A. Sakthivel, K. Jeyasubramanian, S. Seenivasan, J.D. Raja, K. Yun, Removal of hexavalent chromium by biochar derived from Azadirachta indica leaves: batch and column studies. Chemosphere. **286**, 131598 (2022)
28. T.E. Abilio, B.C. Soares, J.C. José, P.A. Milani, G. Labuto, E. Carrilho, N.V.M. Hexavalent chromium removal from water: adsorption properties of in natura and magnetic nanomodified sugarcane bagasse. Environ. Sci. Pollut. Res. **28**, 24816–24829 (2021)
29. N.S. Ammar, N.A. Fathy, H.S. Ibrahim, S.M. Mousa, Micro-mesoporous modified activated carbon from corn husks for removal of hexavalent chromium ions. Appl. Water Sci. **11**, 1–12 (2021)
30. S. Sunkar, P. Prakash, B. Dhandapani, O. Baigenzhenov, J.A. Kumar, V. Nachiyaar, S. Zolfaghari, T. Sara, A. Hosseini-Bandegharaei, Adsorptive removal of acid blue dye 113 using three agricultural waste biomasses: the possibility of valorization by activation and carbonization – a comparative analysis. Environ. Res. **233**, 116486 (2023). https://doi.org/10.1016/j.envres.2023.116486
31. J.A. Kumar, P.S. Kumar, T. Krithiga, D. Prabu, D.J. Amarnath, S. Sathish, D. Venkatesan, A. Hosseini-Bandegharaei, P. Prashant, Acenaphthene adsorption onto ultrasonic assisted fatty acid mediated porous activated carbon-characterization, isotherm and kinetic studies. Chemosphere. **284**, 131249 (2021). https://doi.org/10.1016/j.chemosphere.2021.131249
32. A. Jagadeesan, J. Amarnath, P. Kumar, C. Kaushik, M. Varghese, S. Anbalagan, Mass transfer and thermodynamic analysis on the removal of naphthalene from aqueous solution using oleic acid modified palm shell activated carbon. Desalination Water Treat. **106**, 238–250 (2018). https://doi.org/10.5004/dwt.2018.22066
33. M.J. Ahmed, Preparation of activated carbons from date (Phoenix dactylifera L.) palm stones and application for wastewater treatments. Process Saf. Environ. Prot. **102**, 168–182 (2016)

34. K. Rambabu, A. Thanigaivelan, G. Bharath, N. Sivarajasekar, F. Banat, P.L. Show, Biosorption potential of Phoenix dactylifera coir wastes for toxic hexavalent chromium sequestration. Chemosphere. **268**, 128809 (2021)
35. N. Siva Kumar, M. Asif, A.M. Poulose, E.H. Al-Ghurabi, S.S. Alhamedi, J.R. Koduru, Preparation, Characterization, and Chemically Modified Date Palm Fiber Waste Biomass for Enhanced Phenol Removal from an aqueous environment. Materials. **16** (2023). https://doi.org/10.3390/ma16114057
36. R.A. Nasser, M.Z. Salem, S. Hiziroglu, H.A. Al-Mefarrej, A.S. Mohareb, M. Alam, I.M. Aref, Chemical analysis of different parts of date palm (Phoenix dactylifera L.) using ultimate, proximate and thermo-gravimetric techniques for energy production. Energies. **9**, 374 (2016)
37. H. Yang, R. Yan, T. Chin, D.T. Liang, H. Chen, C. Zheng, Thermogravimetric analysis–fourier transform infrared analysis of palm oil waste pyrolysis. Energy Fuels. **18**, 1814–1821 (2004)
38. K. Wieczorek-Ciurowa, A. Kozak, The thermal decomposition of Fe (NO3) 3· 9H2O. J. Therm. Anal. Calorim. **58**, 647–651 (1999)
39. W. Shaheen, Thermal behaviour of pure and binary Fe (NO3) 3· 9H2O and (NH4) 6Mo7O24· 4H2O systems. Mater. Sci. Engineering: A **445**, 113–121 (2007)
40. H. Wang, P. Hu, D. Pan, J. Tian, S. Zhang, A.A. Volinsky, Carbothermal reduction method for Fe3O4 powder synthesis. J. Alloys Compd. **502**, 338–340 (2010)
41. K. He, Z. Zheng, Z. Chen, Multistep reduction kinetics of Fe3O4 to Fe with CO in a micro fluidized bed reaction analyzer. Powder Technol. **360**, 1227–1236 (2020)
42. W. Liang, G. Wang, C. Peng, J. Tan, J. Wan, P. Sun, Q. Li, X. Ji, Q. Zhang, Y. Wu et al., Recent advances of carbon-based nano zero valent iron for heavy metals remediation in soil and water: a critical review. J. Hazard. Mater. **426**, 127993 (2022). https://doi.org/10.1016/j.jhazmat.2021.127993
43. X. Liu, L. Yang, H. Zhao, W. Wang, Pyrolytic production of zerovalent iron nanoparticles supported on rice husk-derived biochar: simple, in situ synthesis and use for remediation of cr(VI)-polluted soils. Sci. Total Environ. **708**, 134479 (2020). https://doi.org/10.1016/j.scitotenv.2019.134479
44. Y. Fei, N. Han, J. Shi, S. Tang, H. Zhuang, L. Wang, J. Ran, E. Gao, M.A. Habila, Z. Chen et al., Red mud-derived iron carbon catalyst for the removal of organic pollutants in wastewater. Chemosphere. **337**, 139211 (2023). https://doi.org/10.1016/j.chemosphere.2023.139211
45. Q. Zhang, Y. Cheng, C. Fang, J. Chen, H. Chen, H. Li, Y. Yao, Facile synthesis of porous carbon/Fe3O4 composites derived from waste cellulose acetate by one-step carbothermal method as a recyclable adsorbent for dyes. J. Mater. Res. Technol. **9**, 3384–3393 (2020). https://doi.org/10.1016/j.jmrt.2020.01.074
46. M. Jain, M. Yadav, T. Kohout, M. Lahtinen, V.K. Garg, M. Sillanpää, Development of iron oxide/activated carbon nanoparticle composite for the removal of cr(VI), Cu(II) and cd(II) ions from aqueous solution. Water Resour. Ind. **20**, 54–74 (2018). https://doi.org/10.1016/j.wri.2018.10.001
47. X. Jiang, W. Fan, C. Li, Y. Wang, J. Bai, H. Yang, X. Liu, Removal of cr (VI) from wastewater by a two-step method of oxalic acid reduction-modified fly ash adsorption. RSC Adv. **9**, 33949–33956 (2019)
48. R. Vitek, J.C. Masini, Nonlinear regression for treating adsorption isotherm data to characterize new sorbents: advantages over linearization demonstrated with simulated and experimental data. Heliyon. **9**, e15128 (2023). https://doi.org/10.1016/j.heliyon.2023.e15128
49. R. Widiartyasari Prihatdini, A. Suratman, D. Siswanta, Linear and nonlinear modeling of kinetics and isotherm of malachite green dye adsorption to trimellitic-modified pineapple peel. *Materials Today: Proceedings* 2023
50. L.-. Shi, Y.-M. Lin, X. Zhang, Z.-. Chen, Synthesis, characterization and kinetics of bentonite supported nZVI for the removal of cr(VI) from aqueous solution. Chem. Eng. J. **171**, 612–617 (2011). https://doi.org/10.1016/j.cej.2011.04.038
51. L.N. Shi, X. Zhang, Z.L. Chen, Removal of chromium (VI) from wastewater using bentonite-supported nanoscale zero-valent iron. Water Res. **45**, 886–892 (2011). https://doi.org/10.1016/j.watres.2010.09.025
52. Y. Wang, L. Yu, R. Wang, Y. Wang, X. Zhang, A novel cellulose hydrogel coating with nanoscale Fe0 for cr(VI) adsorption and reduction. Sci. Total Environ. **726**, 138625 (2020). https://doi.org/10.1016/j.scitotenv.2020.138625
53. K. Zhu, C. Chen, M. Xu, K. Chen, X. Tan, M. Wakeel, N.S. Alharbi, In situ carbothermal reduction synthesis of Fe nanocrystals embedded into N-doped carbon nanospheres for highly efficient U(VI) adsorption and reduction. Chem. Eng. J. **331**, 395–405 (2018). https://doi.org/10.1016/j.cej.2017.08.126
54. S.K. Mohamed, M. Abuelhamd, N.K. Allam, A. Shahat, M. Ramadan, H.M.A. Hassan, Eco-friendly facile synthesis of glucose–derived microporous carbon spheres electrodes with enhanced performance for water capacitive deionization. Desalination. **477**, 114278 (2020). https://doi.org/10.1016/j.desal.2019.114278
55. V. Gopalakannan, S. Periyasamy, N. Viswanathan, Fabrication of magnetic particles reinforced nano-hydroxyapatite/gelatin composite for selective cr(vi) removal from water. Environ. Science: Water Res. Technol. **4**, 783–794 (2018). https://doi.org/10.1039/C8EW00027A
56. J. Qi, B. Li, P. Zhou, X. Su, D. Yang, J. Wu, Z. Wang, X. Liang, Study on adsorption of hexavalent chromium by composite material prepared from iron-based solid wastes. Sci. Rep. **13**, 135 (2023). https://doi.org/10.1038/s41598-023-27414-9
57. H. Wu, Q. Wu, J. Zhang, Q. Gu, L. Wei, W. Guo, M. He, Chromium ion removal from raw water by magnetic iron composites and Shewanella oneidensis MR-1. Sci. Rep. **9**, 1–16 (2019)
58. P.M. Thabede, N.D. Shooto, T. Xaba, E.B. Naidoo, Magnetite functionalized Nigella sativa seeds for the uptake of chromium (VI) and lead (II) ions from synthetic wastewater. *Adsorption Science & Technology* 2021, *2021*
59. R. He, X. Yuan, Z. Huang, H. Wang, L. Jiang, J. Huang, M. Tan, H. Li, Activated biochar with iron-loading and its application in removing Cr (VI) from aqueous solution. Colloids Surf., a **579**, 123642 (2019)
60. A.E. Ofomaja, E.B. Naidoo, A. Pholosi, Intraparticle diffusion of cr (VI) through biomass and magnetite coated biomass: a comparative kinetic and diffusion study. S. Afr. J. Chem. Eng. **32**, 39–55 (2020)
61. P. Singh, D. Tiwary, I. Sinha, Improved removal of cr (VI) by starch functionalized iron oxide nanoparticles. J. Environ. Chem. Eng. **2**, 2252–2258 (2014)
62. P. Singh, D. Tiwary, I. Sinha, Starch-functionalized magnetite nanoparticles for hexavalent chromium removal from aqueous solutions. Desalination Water Treat. **57**, 12608–12619 (2016)
63. J. Zhu, H. Gu, J. Guo, M. Chen, H. Wei, Z. Luo, H.A. Colorado, N. Yerra, D. Ding, T.C. Ho, Mesoporous magnetic carbon nanocomposite fabrics for highly efficient cr (VI) removal. J. Mater. Chem. A **2**, 2256–2265 (2014)
64. Y. Li, S. Zhu, Q. Liu, Z. Chen, J. Gu, C. Zhu, T. Lu, D. Zhang, J. Ma, N-doped porous carbon with magnetic particles formed in situ for enhanced cr (VI) removal. Water Res. **47**, 4188–4197 (2013)
65. X. Sun, L. Yang, Q. Li, J. Zhao, X. Li, X. Wang, H. Liu, Amino-functionalized magnetic cellulose nanocomposite as adsorbent for removal of cr (VI): synthesis and adsorption studies. Chem. Eng. J. **241**, 175–183 (2014)
66. G. López-Téllez, C.E. Barrera-Díaz, P. Balderas-Hernández, G. Roa-Morales, B. Bilyeu, Removal of hexavalent chromium in

aquatic solutions by iron nanoparticles embedded in orange peel pith. Chem. Eng. J. **173**, 480–485 (2011)
67. Y. Sun, H. Lyu, L. Gai, P. Sun, B. Shen, J. Tang, Biochar-anchored low-cost natural iron-based composites for durable hexavalent chromium removal. Chem. Eng. J. **476**, 146604 (2023). https://doi.org/10.1016/j.cej.2023.146604
68. W. Cheng, J. Wen, W. Yang, Removal of hexavalent chromium using one-step synthesized metal-polyphenol composites epigallocatechin gallate/titanium: performance, interference, and mechanisms. J. Environ. Chem. Eng. **12**, 111866 (2024). https://doi.org/10.1016/j.jece.2023.111866